Compact Broadband Dual-Sense Circularly-Polarized Microstrip Antenna/Array with Enhanced Isolation

Chun-Xu Mao, Steven Gao, Senior Member, IEEE, Yi Wang, Senior Member, IEEE, and Josaphat Tetuko Sri Sumantyo, Senior Member, IEEE

Abstract—This paper presents a novel method of designing the compact dual-sense circularly-polarized (CP) microstrip antenna/array with improved impedance bandwidth, axial ratio (AR) bandwidth and inter-polarization isolation. The left-hand and right-hand CP (LHCP/ RHCP) characteristics are achieved simultaneously by conceiving a vertically coupled resonant structure for the first time. Different from traditional methods, the antenna shows a compact size but exhibits the wide impedance and 3-dB AR bandwidths. For each input, two coupling paths are purposely designed to excite the TM10 and TM01-mode of the patch, respectively. By composing different coupling units in the two paths, an intrinsic ±90º phase difference over a broadband can be obtained, resulting in the broadband CP characteristics. In addition, a novel method of using the neutralization line between the two feeds is investigated to improve the isolation between the polarizations. Based on the dual-sense CP element, a 1 × 4 dual-sense CP array is composed to exemplify its potential applications in large arrays. Compared with traditional CP antennas, the proposed antennas have the advantages of compact size, simplified feed, broad impedance and 3-dB AR bandwidths, and improved isolation. Experimental results verify the predictions.

Index Terms—Broadband, circularly-polarized (CP), compact, dual-sense, isolation, microstrip antenna, array antenna.

I. Introduction

CIRCULARLY polarized (CP) antennas have been widely used in wireless communication systems due to their immunity of orientating the Tx/Rx antennas and the capacity of combating the multipath fading [1]. Dual-sense CP, as one of the diversity techniques, is always used to increase the channel capacity and link robustness [2]-[3]. Usually, the two polarizations are required to have a high isolation so as to improve the diversity performance. To meet the requirements of miniaturization and high data rate in modern portable terminals, the antenna is also required to have a compact size and broad impedance/axial ratio (AR) bandwidths.

A variety of dual-sense CP antennas have been reported in the past years. Dual-sense CP characteristics could be achieved by employing a wide rectangular slot [4] or a dielectric resonator [5] as the radiator. But these antennas suffer from the problems of bi-directional radiation and low gain, thus they are not suitable for array antenna designs. The dual-sense spiral antenna was proposed as the feed of a reflector antenna [6]. However, it has the problems of large volume, heavy weight and high profile. In [7]-[9], dual CP antennas were achieved using the waveguides. Similarly, these antennas have the disadvantages such as bulky structure, high weight, and difficulty for integration. Microstrip antenna is believed to be a candidate to achieve the CP antenna with unidirectional radiation, high gain, low profile and light weight. In [10], a compact CP microstrip patch antenna with wide impedance bandwidth and 3-dB AR bandwidth was proposed by stacking two asymmetrical patches. This method, however, is not suitable to achieve the dual-sense CP antenna and array.

Dual-sense microstrip CP antennas were achieved by using a hybrid coupler [11] or using different feeding modes [12]. However, these traditional methods occupy large footprints and complicated feeding networks are required. Thus, they are not a good candidate in array antenna applications. In addition, these antennas suffer from the narrow impedance and 3-dB AR bandwidths. The dual-sense CP was also achieved by sequentially feeding the cross-shaped slots in the ground [13]-[15]. But the isolation between the two polarizations are always very poor (less than 10 dB). Dual-CP microstrip arrays were achieved by using the sequential rotation techniques [16]-[17]. This technique, however, demands a complex feeding/splitting network and it is not suitable for element design. In [18]-[19], broadband dual-sense CP antennas with a good isolation were reported at the expense of stacked patches, multi-layer feeds and high profile.

In this paper, a novel method is proposed for the first time to achieve the broadband dual-sense CP microstrip antenna element and array with compact size, simplified feed and high isolation. First, the broadband dual-sense CP characteristics were studied by using the topologies of the antenna. The broad impedance and AR bandwidths are realized by employing a

Manuscript submitted on January 31, 2017; This work is supported by UK EPSRC grant EP/N032497/1 and YW is supported by UK EPSRC under Contract EP/M013529/1.

C. X. Mao and S. Gao are with School of Engineering and Digital Arts, University of Kent, CT2 7NZ, UK (email: cm688@kent.ac.uk).

Y. Wang is with the Department of Engineering Science, University of Greenwich, ME4 4TB, UK.

J. Sumantyo is with Center for Environmental Remote Sensing (CEReS), Chiba University, Chiba 263-8522, Japan.

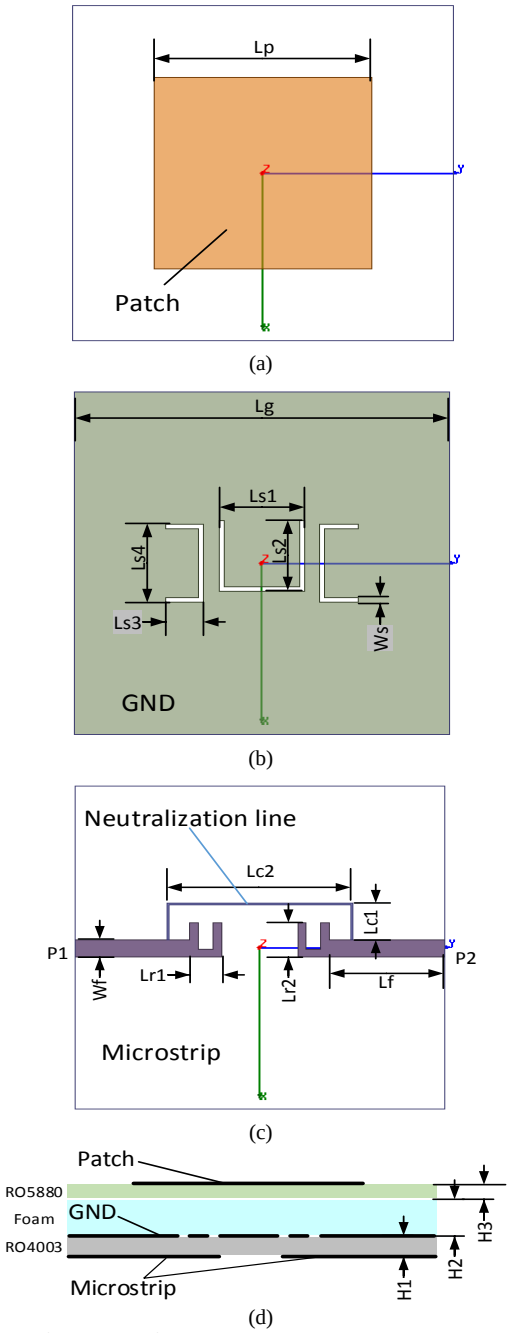

Fig. 1. Configurations of the proposed dual-sense microstrip CP antenna: (a) square patch on the top, (b) ground plane with inserted slots, (c) microstrip lines on the bottom, (d) side-view of the stacked configuration. Lg = 40 mm, Lp = 20 mm, Ls1 = 7.5 mm, Ls2 = 6.5 mm, Ls3 = 3.2 mm, Ls4 = 8 mm, Lr1 = 2.8 mm, Lr2 = 3.6 mm. Lc1 = 5 mm, Lc2 = 18 mm, Ws = 0.5 mm, Lf = 13.2 mm, Wf = 1.8 mm, H1 = 0.8 mm, h2 = 4 mm, h3 = 0.254 mm.

novel vertically coupled resonator-based structure and the intrinsic 90° phase difference between the two coupling paths [20]. Then, a neutralization line is used to improve the isolation between the two polarizations. To verify the concept, an antenna element and a 1 × 4 array were devised and tested. The measured results show that the proposed antenna/array has a good performance in terms of impedance bandwidth, 3-dB AR bandwidth, isolation, and radiation patterns.

This paper is organized as follows. Section II presents the configuration of the proposed antenna and the design methods. Section III illustrates the approaches of improving the isolation. Section IV summarizes the simulated and measured results of the element and the array antenna, followed by conclusions in Section V.

II. Antenna Implementation

A. Configuration

Fig. 1(a)-(d) show the configurations of the proposed broadband dual-sense CP microstrip antenna element. The antenna has a stacked structure. The radiation element is a regular square patch, which is printed on the top layer of the upper substrate, as shown in Fig. 1(a). The dimension of the patch Lp is approximate a half guide wavelength at the designated operation frequency f_0, f_0 = 5.3 GHz. Fig. 1(b) shows the layout of ground plane, which is placed on the top layer of the lower substrate. Three U-shaped slots are inset in the ground plane. The central U-slot has the identical resonant frequency as the patch (f_0). The two U-slots on the both sides, which is shorter than the center one, have a different resonances. The center U-slot is used to excite the TM10-mode of the patch while the lateral slots are used to excite the TM01-mode. It should be noted that the functions of these U-slots are different, which will be detailed in the Part-B.

The feeding networks of the dual-sense CP are printed on the bottom layer of the lower substrate, as shown in Fig. 1(c). A hairpin resonator is integrated at the end of each microstrip line, which also has the same resonance as the patch. The two microstrip feeds are connected using a neutralization line, which is used to improve the isolation between the two polarizations/ports. The operation principles of the neutralization line will be investigated in Section-III.

Fig. 1(d) shows the stacked configuration of the proposed antenna. The patch, U-shaped slots and the feeding networks are stacked and vertically coupled together. Such a structure can not only reduce the antenna size but also significantly improve the impedance and AR bandwidths [21]-[22]. Between the two substrates, a foam with thickness of 4 mm is inserted as a spacer. RO 5880 with a permittivity of 2.2 and loss tangent of 0.0009 is used as the upper substrate while RO 4003C with a permittivity of 3.55 and loss tangent of 0.0027 is used as the lower substrate.

In this work, the patch, central U-slot and hairpins are half-wavelength resonators. All these resonant structures are designed to resonate at the same frequency and vertically coupled to form a 3rd-order resonant circuit, producing a broad impedance bandwidth. These dimensions can be approximately derived using the following equations,

$$Lp \approx \frac{c}{2 f_0 \sqrt{\varepsilon_{eff\,1}}} \quad (1)$$

$$Ls1 + 2 \times Ls2 = \frac{c}{2 f_0 \sqrt{\varepsilon_{eff\,2}}} \quad (2)$$

$$L_{t1} + 2 \cdot L_{t2} \approx \frac{c}{2 f_0 \sqrt{\varepsilon_{eff\,3}}} \quad (3)$$

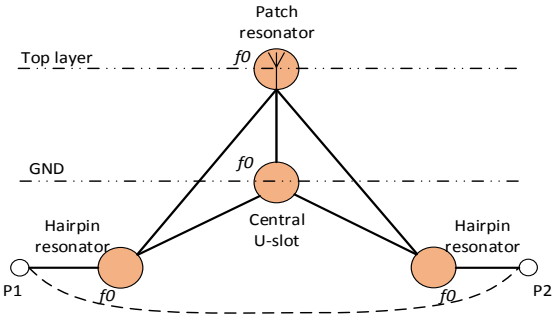

Fig. 2. Resonator-based topology of the proposed dual-sense CP antenna.

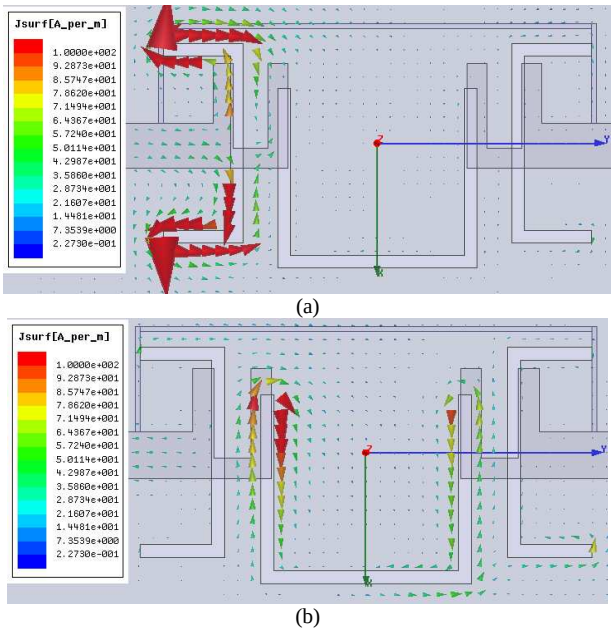

Fig. 3. Current distribution on the ground plane when P1 is excited: (a) t = 0; (b) t = T/4.

where ε_{eff1}, ε_{eff2}, ε_{eff3} are the effective permittivity of patch, slot lines and microstrip, respectively. c is the velocity of light in free space. It should be noted that the length of the hairpin is dramatically different due to the loading effect of the coupling slot. The optimization was performed using the high frequency structural simulator (HFSS 15) and the optimized parameters are also given in the caption of Fig. 1.

B. Generation of dual-sense CP

Since the proposed dual-sense CP antenna consists of multiple resonant units, it can be illustrated using a resonator-based topology, as shown in Fig. 2. The resonators are represented by the circles, whereas the solid lines between them indicate the mutual couplings. The coupling between the resonators can be modelled by an admittance inverter J with an innate and identical 90° phase delay [23]-[24]. As can be observed, the patch, the central U-slot and the hairpins are equivalent to resonators with the same resonance f_0. The two ports (P1, P2) operate at RHCP and LHCP, respectively. These two polarizations share the same patch and the center U-slot. The dash line on the bottom denotes the neutralization line. It should be noted that the two lateral U-slots in Fig. 1 have the different resonances, and thus they are not served as the resonant components here, but the coupling structures.

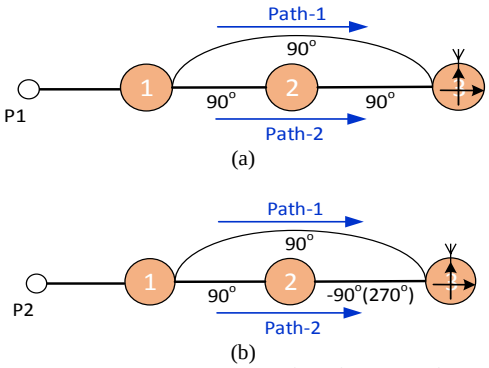

Fig. 4. Resonator-based topologies: (a) left half topology for RHCP; (b) right half topology for LHCP.

These two U-slots are represented by the lines between the patch and the hairpin resonators.

To achieve the CP characteristics, two coupling paths between the hairpin and the patch are purposely devised. The first one is via the U-slot at the center, which is oriented to excite the radiation mode in X-axis direction, TM10-mode. The other is via the lateral U-slot, which is oriented to excite the mode in Y-axis direction, TM01-mode. To produce the required broadband CP, the amplitudes of the two modes should be balanced and with a ±90° phase difference. The amplitudes of the two coupling paths can be controlled by adjusting the relative position between the central slot and the hairpin resonator, denoted as Lf in Fig. 1. On the other hand, due to the two paths contains different coupling units (inverters), the antenna has the intrinsic 90° phase difference over a broadband. Fig. 3 shows the current distribution on the ground plane when P1 is excited. When t = 0, the U-slot on the left is active and strong current flows along the slot, as shown in Fig. 3(a). In contrast, the U-slot at the center is inactive. When t = T/4, as shown in Fig. 3(b), the current around the left U-slot is vanished and strong current emerges around the central U-slot. Where, t and T are the time and the period of a circle, respectively. This current distribution shows that a 90° phase difference is generated between the two coupling paths. It should be noted that the 90° phase difference is originated from the different coupling units along the two transmission paths and thus this innate feature can be applied in a broadband.

The other important contributions of this work is that the LH and RH dual-sense CP can be simultaneously achieved within a compact footprint by elaborately configuring the resonant units and couplings. To illustrate it, the topology in Fig. 2 is split-up along the symmetry axis, generating two 3rd-order resonant circuits, as shown in Fig. 4(a) and (b). It is noted the U-slot resonator at the center and the patch are shared by LHCP and RHCP simultaneously, thus they are regarded as the 2nd and the 3rd resonators of the two circuits. For each polarization, there are two coupling paths from the input to the patch. When P1 is excited, as shown in Fig. 4(a), the first path contains one inverter (90°) whereas the second one contains two inverters (90°+90°). Thus, an inherent phase difference of 90° is obtained, resulting in RHCP. When P2 is excited, as shown in Fig. 4(b), an 180° phase is added

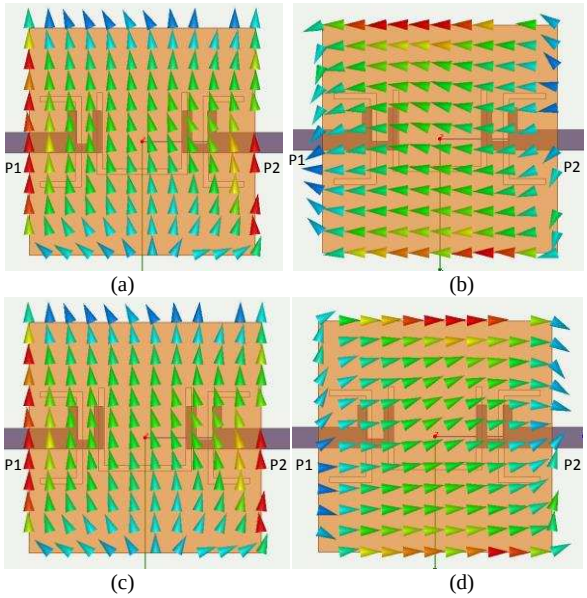

Fig. 5. Simulated current distribution on the patch at 5.4 GHz: (a) t = 0, port-1 is excited, (b) t = T/4, port-1 is excited, (c) t = 0, port-2 is excited (d) t = T/4, port-2 is excited.

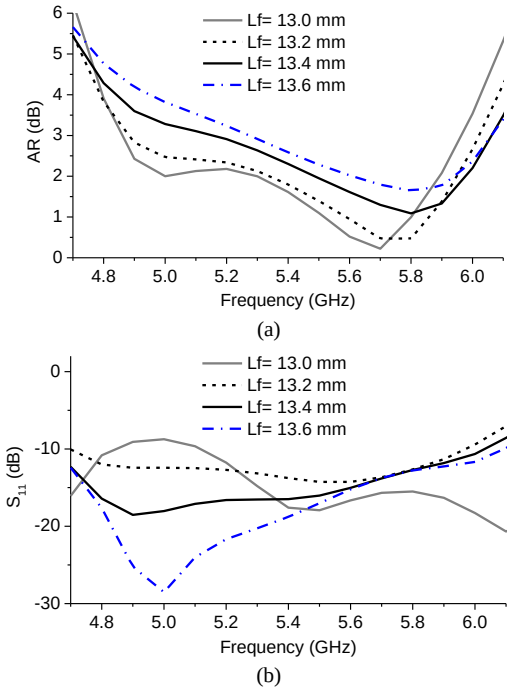

Fig. 6. Simulated results of the proposed antenna with different lengths of the feeds: (a) AR, (b) S-parameters.

between the resonator-2 and patch due to the physical orientation reversal of the central U-slot resonator. As a result, a 270° (-90°) phase is generated between the two coupling paths, resulting in the LHCP.

Fig. 5 shows the simulated current distribution on the patch at 5.4 GHz when P1 and P2 is excited, respectively. When P1 is excited, as can be observed from Fig. 5(a)-(b), the current direction on the patch is changed from –X direction to –Y direction when t changes from 0 to T/4, exhibiting the RHCP characteristics. When P2 is excited, however, the rotation of the current on the patch is reversed, exhibiting the LHCP characteristics, as shown in Fig. 5(c)-(d).

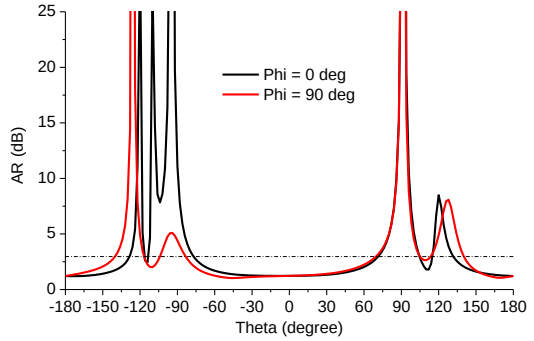

Fig. 7. Simulated AR patterns of the antenna in φ = 0° and 90° planes.

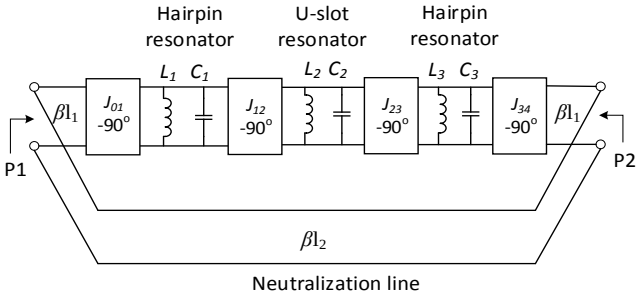

Fig. 8. Equivalent circuit of the two-port feeding network of the antenna.

C. Impedance bandwidth and AR bandwidth

To maintain a good CP characteristic over a broad bandwidth, the two coupling paths are required to have the similar power level. This balance power can be achieved by controlling the coupling strengths between the resonators. In this work, due to the lateral U-slots are perpendicular with the hairpin resonators at the center sections, the path-1 has a stable coupling strength. The coupling strength of the path-2, however, can be controlled by adjusting the distance between the hairpin resonator and the center U-slot. In this way, the two coupling paths can be balanced.

Fig. 6(a)-(b) show the simulated AR and S-parameters of the proposed antenna respectively with the different relative position between the slot and the hairpin, denoted as Lf in Fig. 1. As can be seen from Fig. 6(a), when Lf decreases from 13.6 to 13 mm, the value of AR is reduced and a 3-dB AR bandwidth from 4.85 to 5.95 GHz (FBW = 20%) is achieved. Viewing from Fig. 6(b), the antenna exhibits a broad impedance bandwidth from 4.7 to 5.9 GHz. This broadband characteristic is achieved due to the multi-resonant structure employed in the design. It is observed that the impedance matching is deteriorated as Lf decreases. As a trade-off between the AR and impedance bandwidths, Lf = 13.2 mm was chosen. Fig. 7 shows the simulated AR patterns of the proposed antenna in φ = 0° and 90° planes, respectively. As can be seen, the antenna shows a very good AR performance in the broadside direction with the 3 dB width over 140°.

III. Isolation Improvement

A. Neutralization line

Although the dual-sense CP characteristics are achieved within a compact footprint, the antenna suffers from a poor isolation between the two polarizations/ports. This is mainly

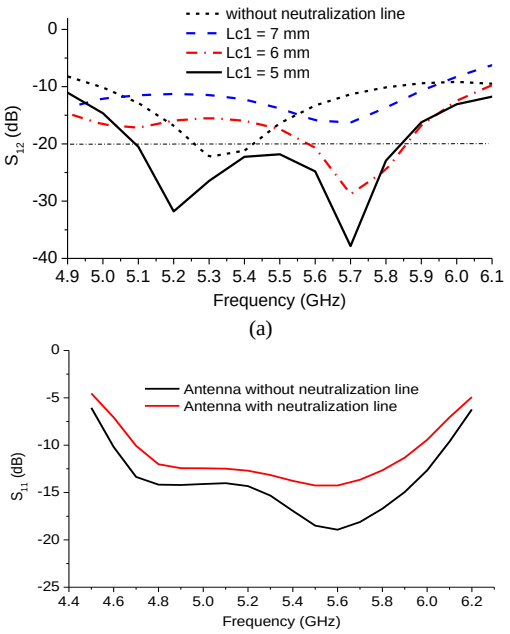

Fig. 9. Comparison of the S-parameters: (a) S_{12} with different lengths of the neutralization line; (b) S_{11} with or without the neutralization line.

attributed to the shared U-slot resonator at the center. As can be observed from Fig. 2, there exists a transmission path between the two hairpin resonators via the central U-slot resonator. This inter-coupling will deteriorate the performance of the polarization diversity. In this section, the method of improving the isolation is investigated.

Fig. 8 shows the equivalent circuit of the two-port feeding network of the proposed antenna (without the patch). The hairpin resonators, U-slot resonator are represented using a shunt LC resonator, while the couplings between the resonators as well as the couplings between the feeds and resonators are modeled using a J-inverter with a phase delay of $\Delta\varphi = 90^{o}$. The neutralization line is modelled using a transmission line with the total length of l_2. There are totally two transmission paths between the two ports. The first one is through the coupled resonators and the other is via the neutralization line. Based on the equivalent circuit, the total phase delays of the two paths can be approximately calculated,

$$\varphi_{\text{total-1}} = 2\cdot\beta\cdot l_1 + 4\cdot\Delta\varphi \quad (4)$$

$$\varphi_{\text{total-2}} = \beta\cdot l_2 \quad (5)$$

$$l_2 = 2\cdot \text{Lc1} + \text{Lc2} \quad (6)$$

where $\varphi_{\text{total-1}}$ and $\varphi_{\text{total-2}}$ are the total phase delays of the transmission path-1 and path-2, respectively, l_1 is the distance between the junction and the hairpin resonator, l_2 is the total length of the neutralization line.

To cancel the coupled electromagnetic components at the output and improve the isolation between the two ports, the phase delays of the two transmission paths should be reversed at the junction of the output,

$$\varphi_{\text{total-1}} - \varphi_{\text{total-2}} \approx \pi \quad (7)$$

This equation can be realized by adjusting the length of the neutralization line. Fig. 9 compares the simulated S-parameters of the antenna with and without the neutralization line. As can be seen from Fig. 9(a), the antenna without the neutralization line shows a good isolation performance only in a narrow band with a pole observed at around 5.35 GHz. The isolation is dramatically deteriorated as the frequency moves to the lower or higher bands. When the neutralization line is employed in this work, an additional pole is introduced and which moves to the higher band as the Lc1 decreases, resulting in a broadband improved isolation performance. When Lc1 = 5 mm, two poles are observed at 5.2 and 5.7 GHz, respectively, producing a wideband isolation over 20 dB from 5.1 to 5.85 GHz. Although the neutralization line is beneficial to improve the isolation, it has a slight effect on the performance of the S_{11}, as shown in Fig. 9(b). The reflection coefficient increases by about 2 dB in the designated band.

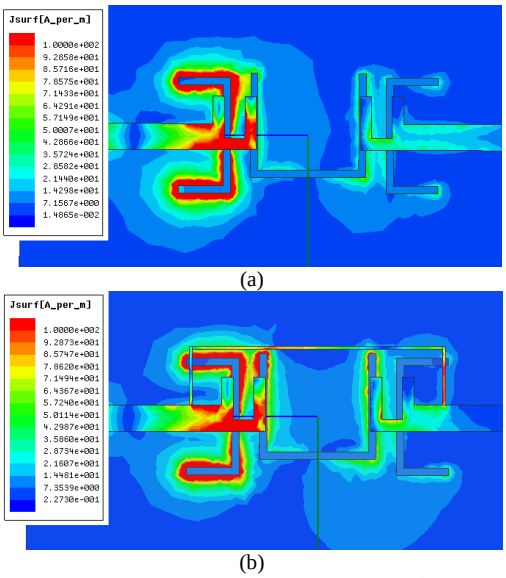

Fig. 10. Current distribution on the ground and the feed lines of the proposed dual-sense CP antenna when P1 is excited: (a) without neutralization line, (b) with neutralization line.

B. Current distribution

Fig. 10 compares the simulated current distribution on the ground and feed lines of the proposed dual-sense CP antenna when P1 is excited. As can be seen from Fig. 10(a), strong current emerges on the feed of P2 when the neutralization line is removed, indicating a poor isolation between the two ports. When the neutralization line is introduced, as shown in Fig. 10(b), a strong current is emerged on the neutralization line and the current on the P2 is significantly reduced, showing an improved isolation between the two ports.

To explain the mechanism for improving the isolation, the current magnitude as well as the phase features on the feed and the neutralization line are presented in Fig. 11. It is observed that there is strong current on the feed line and the neutralization line, as shown in Fig. 11(a). At the junction section, the current from the feed flows into the junction, while the current from the neutralization line flows out. This reversed current component introduced from the neutralization results in the cancelation of the current at the junction and therefore the output. When the neutralization line is removed, as shown in Fig. 11(b), the current on the feed directly transfers to the output, leading to a poor isolation between the two ports/polarizations.

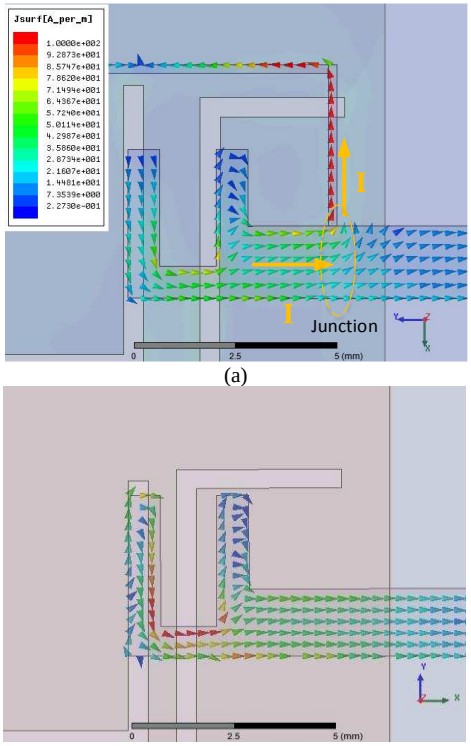

(a)

(b)

Fig. 11. Simulated current distribution on the feed of the LHCP (P2) when RHCP (P1) is excited: (a) with neutralization line, (b) without neutralization line.

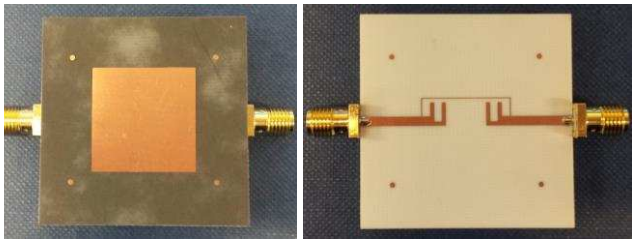

Fig. 12. Prototype of the broadband dual-sense CP antenna element: (a) front view, (b) back view.

IV. Prototypes and Results

A. Dual-sense CP antenna element

The proposed broadband dual-sense CP antenna element was fabricated and the prototype is shown in Fig. 12. The antenna was measured using Anritsu 37397C vector network analyzer. Fig. 13 shows the simulated and measured S-parameters of the antenna element. Thanks to the symmetry, the antenna has the similar impedance characteristics for the two polarizations. The measured impedance bandwidth is from 4.7 to 6.15 GHz (FBW = 26.8%), which is slightly wider than the simulations. The antenna also exhibits the high isolation from 5 to 5.9 GHz with the measured S_{12} below to -17 dB in the band. The discrepancy between the measured and simulated results is attributed to the fabrication and assembly tolerances.

Fig. 14(a)-(b) show the simulated and measured AR of the proposed dual-sense CP antenna element in the broadside direction when P1 and P2 are excited, respectively. Owing to the symmetry, the antenna exhibits the consistent AR

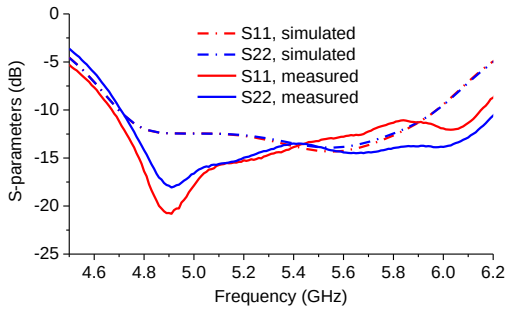

(a)

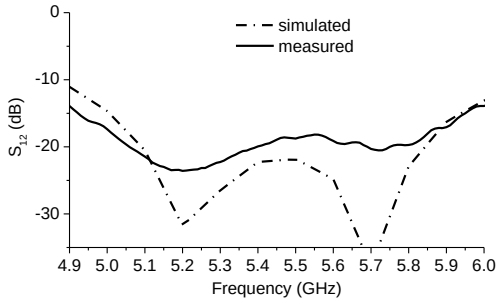

(b)

Fig. 13. Simulated and measured S-parameters of the proposed broadband dual-sense CP antenna element: (a) reflection coefficient, (b) S_{12}.

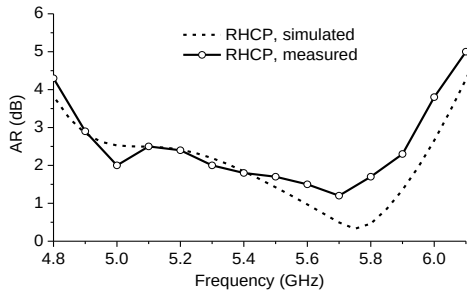

(a)

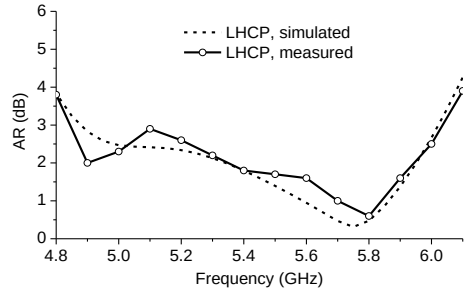

(b)

Fig. 14. Simulated and measured AR of the proposed dual-sense CP antenna element: (a) port-1 is excited, RHCP, (b) port-2 is excited, LHCP.

characteristics when the two polarizations/ports are excited. The measured 3-dB AR bandwidths of the RHCP and LHCP are from 4.9 to 5.95 GHz and 4.85 to 6 GHz, respectively. The measured results agree reasonably well with the simulations.

Fig. 15 shows the simulated and measured normalized radiation patterns of the proposed dual CP antenna element at 5.4 GHz when P1 is excited. The measured results agree well with the simulations, showing a good RHCP radiation performance with the maxima in the broadside direction. The measured cross polarization discrimination (XPD) in the two orthogonal planes are over 20 dB. The discrepancy is mainly

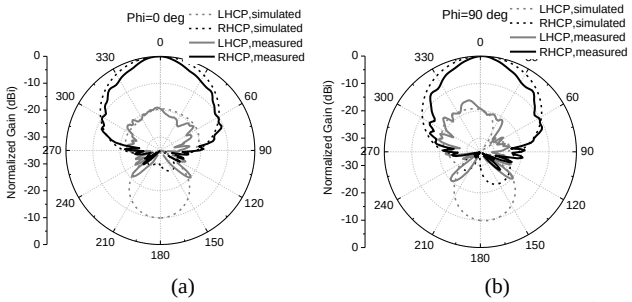

(a) (b)

Fig. 15. Measured and simulated normalized radiation patterns of the antenna element at 5.4 GHz when P1 is excited: (a) φ = 0º, (b) φ = 90º.

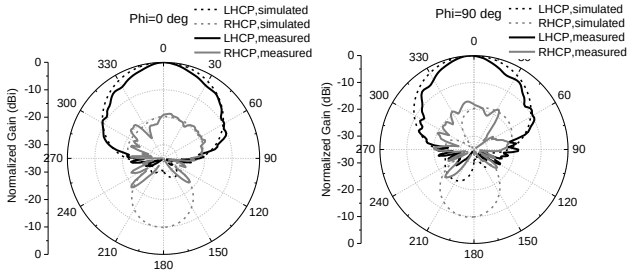

(a) (b)

Fig. 16. Measured and simulated normalized radiation patterns of the antenna element at 5.4 GHz when P2 is excited: (a) φ = 0º, (b) φ = 90º.

caused by measurement tolerance. Fig. 16 shows the simulated and measured normalized radiation patterns in the two orthogonal planes when P2 is excited. In contrast, the antenna exhibits the LHCP radiation in the broadside direction with the XPD over 18 dB. Due to the intrinsic radiation characteristics of the slot couplings and hairpin resonators, the antenna suffers from a problem of the backward radiation in a broadband.

B. Dual-sense CP array antenna

Owing to its compactness, the proposed dual-sense CP element is very suitable for the large array applications. As a proof-of-concept, a 1 × 4 small array is constructed here, as the prototype shown in Fig. 17. The proposed antenna has a small distance of 30 mm (0.53 wavelength at 5.3 GHz) between the elements for reducing the side-lobes of the array. To reduce the potential congestion of the feeding network in a large array, the serial-feed method is exemplified here. The transmission lines between two adjacent elements are bent to meet the 360º phase delay (around 33 mm). Fig. 18 shows the simulated and measured S-parameters of the proposed array antenna. Due to the symmetry, the antenna has a consistent reflection coefficients at the two ports (polarizations). The impedance bandwidth is measured from 4.65 to 5.9 GHz (FBW = 25%), which is slightly wider than the simulations. An excellent isolation of over 19 dB is achieved from 4.7 to 5.85 GHz. The minor discrepancy between the measured and simulated results is caused by fabrication tolerances.

Fig. 19(a)-(b) show the simulated and measured AR of the proposed dual-sense CP antenna array in the broadside direction when P1 and P2 are excited, respectively. The measured 3-dB AR bandwidth is from 4.9 to 5.5 GHz when P1 is excited (RHCP radiation). When P2 is excited (LHCP radiation), the 3-dB AR bandwidth is measured from 4.9 to 5.55 GHz. The measured results are slightly higher than the

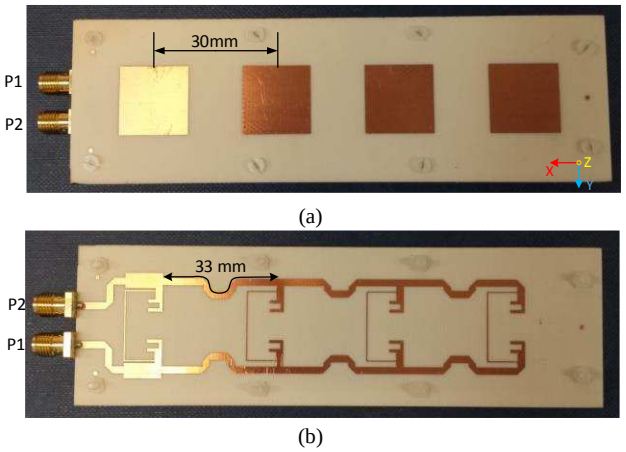

(a)

(b)

Fig. 17. Prototype of the dual-sense CP antenna array: (a) front view, (b) back view.

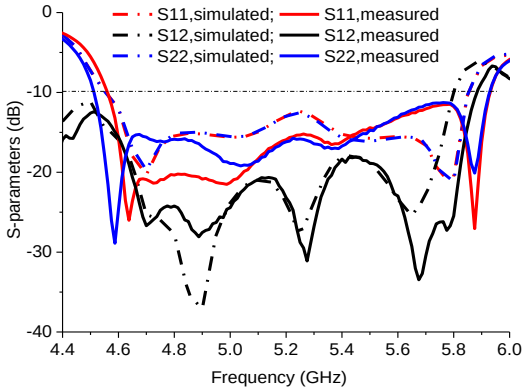

Fig. 18. Simulated and measured S-parameters of the proposed broadband dual-sense CP antenna array.

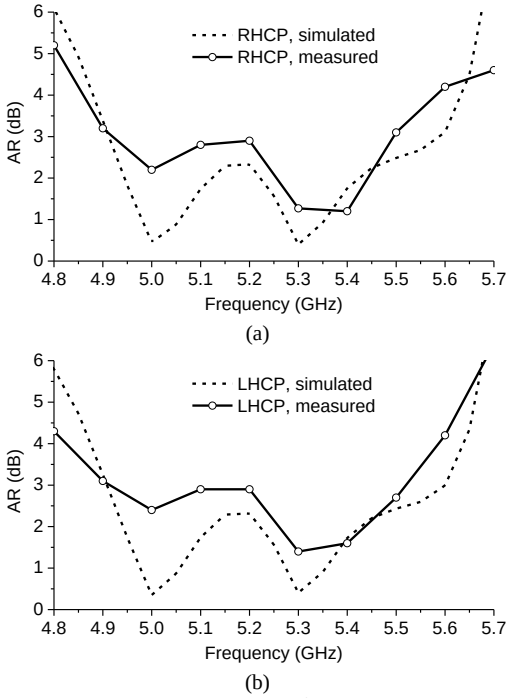

(a)

(b)

Fig. 19. Simulated and measured AR of the proposed dual-sense CP antenna array: (a) port-1 is excited, RHCP, (b) port-2 is excited, LHCP.

simulations, which may be caused by the assembly and measurement tolerances.

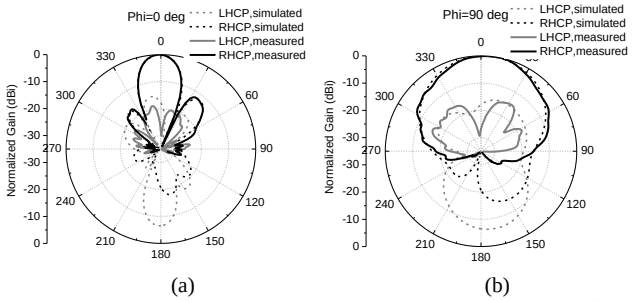

(a) (b)

Fig. 20. Measured and simulated normalized radiation patterns of the antenna array at 5.3 GHz when P1 is excited: (a) φ = 0°, (b) φ = 90°.

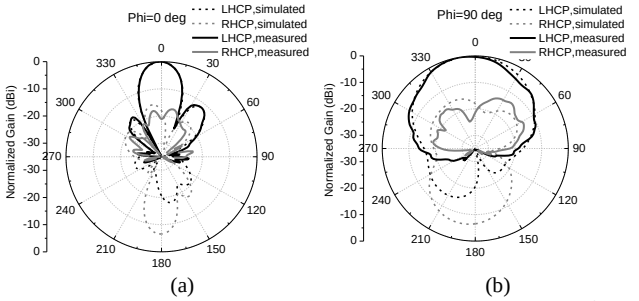

(a) (b)

Fig. 21. Measured and simulated normalized radiation patterns of the antenna array at 5.3 GHz when P2 is excited: (a) φ = 0°, (b) φ = 90°.

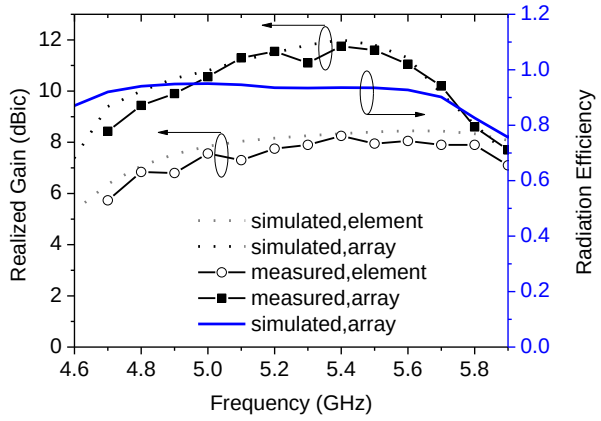

Fig. 22. Measured and simulated antenna gains of the proposed antenna element and array as well as the simulated radiation efficiency of the array.

Fig. 20 shows the simulated and measured normalized radiation patterns of the proposed dual CP array antenna at 5.3 GHz when P1 is excited. The measured results agree well with the simulations, showing that the antenna has a good RHCP radiation performance in the broadside direction. The measured XPD in the two orthogonal planes are over 25 dB. The discrepancy of the backwards radiations is mainly caused by blockage of the measurement devices. Fig. 21 shows the simulated and measured normalized radiation patterns at 5.3 GHz when P2 is excited. Reversely, the antenna exhibits the LHCP radiation in the broadside direction with the XPD over 20 dB.

The simulated and measured gains of the proposed antenna element and array are shown in Fig. 22. Both the element and array have the stable gain responses over a broadband from 4.9 to 5.7 GHz. At the center frequency 5.3 GHz, the gains of the element and array are around 7.9 and 11.3 dBic, respectively. The simulated results also show that the antenna array has a high radiation efficiency over 90% in the designated bands.

Table I compares the proposed dual-sense CP antenna with other reported methods of achieving the dual-sense microstrip CP antennas in [11]-[12], [14] and [16]. This comparison mainly focuses on the realization method, antenna size, thickness, impedance bandwidth, AR bandwidth and isolation between the two ports/polarizations. Compared with the antennas in [11] and [12], the impedance, 3-dB AR bandwidths, and isolation are significantly increased. The antennas in [14] and [16] have the good bandwidths, but they suffer from large element dimension or poor port isolation. For the proposed antennas, though the antenna element has the similar size as the other reported works, the size can be significantly reduced when it is used to conceive an array antenna. The isolations of the proposed element and array are higher than 17 and 19 dB, both of which are much higher than the reported dual-sense CP antennas/arrays.

V. Conclusion

This paper proposes an entirely new technique to realize the compact dual-sense CP microstrip antenna/array over a broadband. By introducing two coupling paths, two orthogonal CP characteristics are achieved without using the traditional power dividers and phase shifters. In addition, the isolation between the two polarizations is improved by employing a neutralization technique between the two ports. A 1 × 4 array antenna is conceived based on the proposed element to exemplify its potential applications in array antenna designs. Compared with traditional dual-sense CP antenna, the proposed antenna exhibits the compact size, improved impedance bandwidth, 3-dB AR bandwidth, and isolation between the ports/polarizations.

References

[1] S. Gao, Q. Luo and F. Zhu, “Circularly polarized antennas,” Hoboken, NJ, USA: Wiley, 2013.

TABLE I
COMPARISON WITH OTHER REPORTED DUAL-SENSE MICROSTRIP CP ANTENNAS

Antennas	Realization method	Thickness	Element size	Impedance bandwidth	3-dB AR bandwidth	Isolation (dB)	XPD (dB)
[11]	hybrid coupler	0.073λ	0.7λ × 0.7λ	2.3%	2.0%	10	15
[12]	different excitation modes	0.026λ	0.7λ × 0.75λ	3.2%	1.1%	10	14
[14]	sequentially feed cross-slot	0.210λ	0.94λ × 0.94λ	23.0%	13.5%	11	20
[16]	sequentially rotation	0.057λ	-	16.0%	14.8%	10	17
This work	element	0.091λ	0.7λ × 0.7λ	26.8%	19.4%	17	18
	array	0.091λ	0.54λ × 0.54λ	25.0%	11.5%	19	19

[2] E. Casini, K. P. Liolis, J. Vilardeboo, and A. I. Neira, "Statistical modeling of dual-polarized MIMO land mobile satellite channels," IEEE Trans.Commun., vol. 58, no. 11, pp. 3077–3083, Nov. 2010.

[3] P. Arapoglou, K. Liolis, M. Bertinelli, A. Panagopoulos, P. Cottis, and R. De Gaudenzi, "MIMO over satellite: A review," IEEE Commun. Surv. Tuts., vol. 13, no. 1, pp. 27–51, 1st Quart. 2011.

[4] R. K. Saini and S. Dwari, "A broadband dual circularly polarized square slot antenna," IEEE Trans. Antennas Propag., vol. 64, no. 1, pp. 290–294, Jan. 2016.

[5] L. Lu, Y. C. Jiao, W. Liang and H. Zhang, "A novel low-profile dual circularly polarized dielectric resonator antenna," IEEE Trans. Antennas Propag., vol. 64, no. 9, pp. 4078–4083, Sep. 2016.

[6] A. Mehrabani and L. Shafai, "Compact dual circularly polarized primary feeds for symmetric parabolic reflector antennas," IEEE Antennas Wireless Propag. Lett., vol. 15, pp. 922-925, 2016.

[7] C. Kumar, V. V. Srinivasan, V. K. Lakshmeesha and S. Pal, "Novel dual circularly polarized radiating element for spherical phased-array applications," IEEE Antennas Wireless Propag. Lett., vol. 8, pp. 826-829, 2009.

[8] Y. Cai, Y. Zhang, Z. Qian W. Cao and S. Shi, "Compact wideband dual circularly polarized substrate integrated waveguide horn antenna," IEEE Trans. Antennas Propag., vol. 64, no. 7, pp. 3184–3189, Jul. 2016.

[9] K. Sakakibara, Y. Kimura, J. Hirokawa, M. Ando, N. Goto, "A two-beam slotted leaky waveguide array for mobile reception of dual-polarization DBS," IEEE Trans. Antennas Propag., vol. 48, no. 1, pp. 1–7, Jan. 1999.

[10] Nasimuddin, X. Qing, Z. N. Chen, "A wideband circularly polarized stacked slotted microstrip patch antenna," IEEE Antennas Propag. Magazine, vol. 55, no. 6, pp. 84-99, Jun. 2013.

[11] X. Bai, X. Liang, M. Li, B. Zhou, J. Geng and R. Jin, "Dual-circularly polarized conical-beam microstrip antenna," IEEE Antennas Wireless Propag. Lett., vol. 14, pp. 482-485, 2015.

[12] A. Narbudowicz, X. Bao and M. Ammann, "Dual circularly-polarized patch antenna using even and odd feed-line modes," IEEE Trans. Antennas Propag., vol. 61, no. 9, pp. 4828–4831, Sep. 2013.

[13] E. Aloni and R. Kastner, "Analysis of a dual circularly polarized microstrip antenna fed by crossed slots," IEEE Trans. Antennas Propag., vol. 42, no. 8, pp. 1053–1058, Aug. 1994.

[14] C. Zhang, X. Liang, X. Bai, J. Geng and R. Jin, "A broadband dual circularly polarized patch antenna with wide beamwidth," IEEE Antennas Wireless Propag. Lett., vol. 13, pp. 1057-1060, 2014.

[15] Z. Harouni, L. Cirio, L. Osman, A. Gharsallah and O. Picon, "A dual circularly polarized 2.45-GHz rectenna for wireless power transmission," IEEE Antennas Wireless Propag. Lett., vol. 10, pp. 306-309, 2011.

[16] Y. Shen, S. G. Zhou, G. L. Huang and T. H. Chio, "A compact dual circularly polarized microstrip patch array with interlaced sequentially rotated feed," IEEE Trans. Antennas Propag., vol. 64, no. 11, pp. 4933–4936, Nov. 2016.

[17] Q. Luo, S. Gao, M. Sobhy, J. T. S. Sumantyo, J. Li, G. Wei, J. Xu, and C. Wu, "Dual circularly polarized equilateral triangular patch array," IEEE Trans. Antennas Propag., vol. 64, no. 6, pp. 2255–2262, Jun. 2016.

[18] A. Garcia, J. M. Inclan, L. Vigil, J. M. Fernandez and M. Sierra, "Low-profile dual circularly polarized antenna array for satellite communications in the X band," IEEE Trans. Antennas Propag., vol. 60, no. 5, pp. 2276–2284, May. 2012.

[19] S. Ye, J. Geng, X. Liang, Y. Guo, R. Jin, "A compact dual-band orthogonal circularly polarized antenna array with disparate elements," IEEE Trans. Antennas Propag., vol. 63, no. 4, pp. 1359–1364, Apr. 2015.

[20] C. X. Mao, S. Gao, Y. Wang, Q. X. Chu, X. X. Yang, "Dual-band circularly-polarized shared-aperture array for C/X-band satellite communications," IEEE Trans. Antennas Propag., vol. 65, no. 10, pp. 5171–5178, Oct. 2017.

[21] C. X. Mao, S.Gao, Y. Wang, "Broadband high-gain beam-scanning antenna array for millimeter-wave applications," IEEE Trans. Antennas Propag., vol. 65, no. 9, pp. 4864 - 4868, Sep. 2017.

[22] C. X. Mao, S.Gao, Y. Wang, F. Qin, Q. X. Chu, "Multimode resonator-fed dual-polarized antenna array with enhanced bandwidth and selectivity," IEEE Trans. Antennas Propag., vol. 63, no. 12, pp. 5492-5499, Dec. 2015.

[23] J. S. Hong and M. J. Lancaster, Microwave Filger for RF/Microwave Application. New York: Wiley, 2001.

[24] C. K. Lin, S. J. Chung, "A filtering microstrip antenna array," IEEE Trans. Microw. Theory Techn., vol. 59, pp. 2856-2863, 2011.

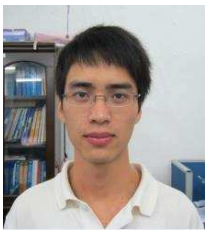

Chun-Xu Mao was born in Hezhou, Guangxi, China. He received the M.S. degree in RF and microwave engineering from South China University of Technology in 2013. He is currently working toward the Ph.D. degree at University of Kent, U.K. His research interests include UWB antenna, filtering antenna, circularly-polarized antenna, integration of passive devices, antenna array for satellite communication and space-borne synthetic aperture radar.

Steven (Shichang) Gao (M'01–SM'16) is a Professor and Chair of RF and Microwave Engineering at University of Kent, UK. His research covers smart antennas, phased arrays, MIMO, satellite antennas, RF/microwave/mm-wave circuits, satellite communications, UWB radars, synthetic-aperture radars and mobile communications. He has two books including <<Space Antenna Handbook>> (Wiley, 2012) and <<Circularly Polarized Antennas>> (IEEE-Wiley, 2014), over 200 papers and several patents. He is an IEEE AP-S Distinguished Lecturer, an Associate Editor of IEEE Transactions on Antennas and Propagation, an Associate Editor of Radio Science and the Editor-in-Chief for Wiley Book Series on "Microwave and Wireless Technologies". He was General Chair of LAPC 2013, and a Keynote Speaker or Invited Speaker at some international conferences such as AES'2014 (China), IWAT'2014 (Sydney), SOMIRES'2013 (Japan), APCAP'2014 (China), etc.

Yi Wang (M'09–SM'12) received the B.Sc. degree in Physics and M.Sc. degree in Condensed Matter Physics from the University of Science and Technology, Beijing, China, in 1998 and 2001, respectively, and the Ph.D. degree in Electronic and Electrical Engineering from The University of Birmingham, in 2005. In 2011, he became a Senior Lecturer at the University of Greenwich in the UK. His present research interests include millimetre-wave/terahertz devices for metrology, communications and sensors, microwave circuits based on multi-port filtering networks, and antennas.

Josaphat Tetuko Sri Sumantyo (S'00-M'04-SM'12) was born in Bandung, Indonesia in 1970. He received the B.Eng. and M.Eng. degrees in electrical and computer engineering from Kanazawa University, Japan, in 1995 and 1997, respectively, and the Ph.D. degree in artificial system sciences from Chiba University, Chiba, Japan, in 2002. In 2000, he was with the Center for Environmental Remote Sensing, Chiba University, as a Research Assistant, and he was a Lecturer from 2002 to 2005. He is currently a full Professor and Head in the Josaphat Microwave Remote Sensing Laboratory (JMRSL), Center for Environmental Remote Sensing, Chiba University. His main interests include analysis of printed antennas and parabolic antennas for mobile satellite communications and synthetic aperture radar (SAR), scattering wave analysis and its applications in microwave remote sensing. Prof. Sri Sumantyo is also a Member of the IEICE, JSPRS, and RSSJ. He is the recipient of many awards and research grants and he published 11 books and more than 670 papers in journals, conferences and invited talks.